applied sciences

MDPI

Article

Lifting-Line Predictions for the Ideal Twist Effectiveness of Spanwise Continuous and Discrete Control Surfaces †

Zachary S. Montgomery [1], Douglas F. Hunsaker [1,*] and James J. Joo [2]

[1] Mechanical and Aerospace Engineering, Utah State University, Logan, UT 84322, USA; zach.montgomery@usu.edu
[2] U.S. Air Force Research Laboratory, Wright-Patterson Air Force Base (WPAFB), Dayton, OH 45433, USA; james.joo.1@us.af.mil
* Correspondence: doug.hunsaker@usu.edu
† Presented as paper 2020–2008 at the AIAA SciTech 2020 Forum, Orlando, FL, USA, 6–10 January 2020.

Featured Application: Preliminary design analysis of novel or traditional control surfaces/mechanisms used to minimize induced drag in multiple flight conditions.

Abstract: Modern materials and manufacturing technologies have allowed the construction of morphing wings that are able to continuously vary certain airfoil parameters such as twist, camber, or control surface deflection as a function of span. This work presents a twist effectiveness parameter as a means of comparing the ideal aerodynamic efficiency of spanwise continuous control surfaces (morphing wings) and spanwise discrete control surfaces (standard wings). A numerical algorithm is used to compute the twist effectiveness of both continuous and discrete control-surface designs over a wide range of planform shapes with evenly spaced actuation for inviscid, incompressible flow. Results included here show that using continuous control surfaces instead of discrete control surfaces reduces induced drag by less than 5% for most applications.

Keywords: lifting-line; twist; optimization; continuous control surfaces; morphing wings; aerodynamic efficiency; MachUp

check for updates

Academic Editors: Yue Zhang and Zhenlong Wu

Received: 13 January 2025
Revised: 27 February 2025
Accepted: 12 March 2025
Published: 19 March 2025

Citation: Montgomery, Z.S.; Hunsaker, D.F.; Joo, J.J. Lifting-Line Predictions for the Ideal Twist Effectiveness of Spanwise Continuous and Discrete Control Surfaces. *Appl. Sci.* **2025**, *15*, 3383. https://doi.org/10.3390/app15063383

Copyright: © 2025 by the authors. Licensee MDPI, Basel, Switzerland. This article is an open access article distributed under the terms and conditions of the Creative Commons Attribution (CC BY) license (https://creativecommons.org/licenses/by/4.0/).

1. Introduction

Wing twist can be used to control the lift distribution on a wing. In general, twist can be categorized as either geometric or aerodynamic. Geometric twist is a spanwise variation in geometric angle of attack. A common form of geometric twist is washout, which is a twisting of the wing to reduce the angle of attack near the wing tips. Aerodynamic twist is a spanwise variation in zero-lift angle of attack. A common form of aerodynamic twist is a flap that extends over only a portion of the wing. In either scenario, wing twist always results in a spanwise variation in the section angle of attack relative to the section zero-lift angle of attack. Twist can be defined as

$$T(z) \equiv \alpha(z) - \alpha_{L0}(z) - (\alpha - \alpha_{L0})_{\text{root}} \tag{1}$$

where the components $\alpha(z) - \alpha_{\text{root}}$ and $-\alpha_{L0}(z) + \alpha_{L0\ \text{root}}$ are the contributions from the local geometric and aerodynamic twist, respectively.

Any form of twist can be applied in a spanwise continuous or discontinuous manner. For example, washout is usually a continuous form of twist, while flaps are a discontinuous form of twist. The original Wright flyer used geometric continuous twist, referred to

as wing warping, for roll control [1,2], but later models switched to discrete flaps for structural reasons. Most aircraft today use discontinuous twist in the form of flaps to control the lift distribution and resultant forces and moments, likely due to structural simplicity. However, with modern morphing technology, it is now possible to accurately control a continuous twist distribution (aerodynamic or geometric) during flight. For example, AFRL [3], NASA [4–7], and others [8–13] have developed various methods for varying the camber along a wing during flight, with an emphasis on maintaining continuity of twist along the span.

The main benefit claimed by those employing continuous twist control rather than discontinuous twist control is a reduction in drag over the flight envelope, and studies have reported varying levels of drag benefits [4,7,14–23]. In order to adequately quantify the drag benefits of real-time continuous twist, a consistent and rigorous methodology for drag comparison must be employed. Studies for comparing induced drag, parasitic drag, and total drag of various discrete and continuous designs must be conducted. Here, we provide one sample methodology and evaluate the induced-drag benefits of wings with continuous twist control compared to wings with discrete twist control.

Wings with mechanisms that control the twist distribution in a spanwise continuous manner are defined here as having a continuous control surface. In contrast, wings with mechanisms that vary the twist at discrete spanwise sections are defined here as having discrete control surfaces. Figure 1 visually indicates the difference between spanwise discrete and continuous control surfaces. Here, we use a numerical potential flow algorithm to evaluate ideal induced-drag solutions over a wide range of wing planforms and control mechanism designs. Comparisons are made between continuous and discrete control surfaces for comparable wing planforms and degrees of freedom within the respective control mechanisms. These results can aid in preliminary design of wings that use active control to minimize induced drag over the flight envelope. While the results presented here are limited to spanwise-symmetric planforms and twist distributions, and therefore spanwise-symmetric lift distributions, the method could be applied to asymmetric scenarios.

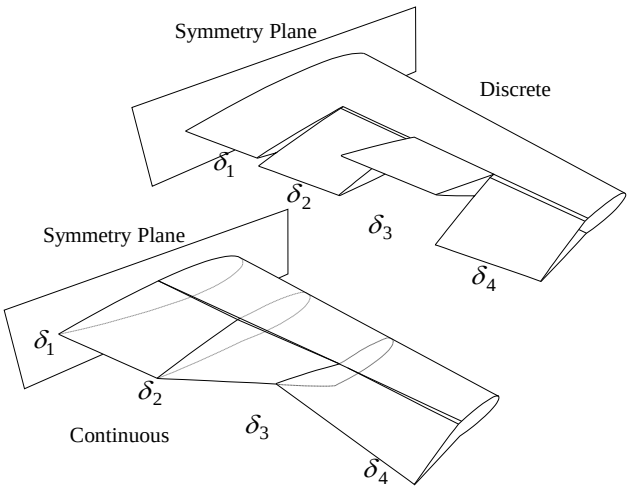


Figure 1. Visual comparing spanwise discrete and continuous control surface types.

2. Materials and Methods

2.1. Theoretical Development

The prevailing theory that relates wing planform, twist, and angle of attack to the resulting lift and induced drag is the classical lifting-line theory published by Prandtl in 1918 [24,25]. Phillips presented a much more useful form of lifting-line theory which

provides significant insight into these relationships [26–29]. The following development is an overview of that formulation. The solution to the fundamental lifting-line equation gives the vortex strength of the lifting line as a Fourier sine series:

$$\Gamma(\theta) = 2bV_\infty \sum_{n=1}^{N} A_n \sin(n\theta), \qquad \theta \equiv \cos^{-1}\left(-\frac{2z}{b}\right) \tag{2}$$

where θ is a change in variables for the spanwise coordinate. The lift and induced-drag coefficients as functions of the Fourier coefficients in the absence of rolling rate are

$$C_L = \pi R_A A_1 \tag{3}$$

$$C_{D_i} = \pi R_A \sum_{n=1}^{N} n A_n^2 \tag{4}$$

In order to decouple the effects of angle of attack and twist, a change in variables can be used as suggested by Phillips [26–28]. A similar change in variables is used here, given by

$$A_n \equiv a_n(\alpha - \alpha_{L0})_{\text{root}} + b_n\Omega \tag{5}$$

where the decomposed Fourier coefficients a_n and b_n are related to the wing planform and twist distribution according to

$$\sum_{n=1}^{N} a_n \left[\frac{4b}{\widetilde{C}_{L,\alpha}c(\theta)} + \frac{n}{\sin(\theta)}\right] \sin(n\theta) = 1 \tag{6}$$

$$\sum_{n=1}^{N} b_n \left[\frac{4b}{\widetilde{C}_{L,\alpha}c(\theta)} + \frac{n}{\sin(\theta)}\right] \sin(n\theta) = \omega(\theta) \tag{7}$$

The term Ω is the amount of twist at the location of maximum twist magnitude of the wing and $\omega(\theta)$ is the twist distribution function normalized by Ω. The twist distribution function $\omega(\theta)$ determines the shape of the twist distribution, while Ω determines the amount of twist. The twist distribution is then given as

$$T(\theta) = \Omega\omega(\theta) \tag{8}$$

Using Equations (5)–(7) in Equation (4) gives the induced-drag coefficient for a wing with an arbitrary $c(\theta)$, $\omega(\theta)$, and Ω, as

$$C_{D_i} = \frac{C_L^2(1+\kappa_P) + \kappa_{PL}C_L C_{L.\alpha}\Omega + \kappa_{P\Omega}(C_{L,\alpha}\Omega)^2}{\pi R_A} \tag{9}$$

where

$$\kappa_P = \sum_{n=2}^{N} n\frac{a_n^2}{a_1^2} \tag{10}$$

$$\kappa_{PL} = 2\frac{b_1}{a_1}\sum_{n=2}^{N} n\frac{a_n}{a_1}\left(\frac{b_n}{b_1} - \frac{a_n}{a_1}\right) \tag{11}$$

$$\kappa_{P\Omega} = \left(\frac{b_1}{a_1}\right)^2 \sum_{n=2}^{N} n\left(\frac{b_n}{b_1} - \frac{a_n}{a_1}\right)^2 \tag{12}$$

For a given section lift slope, the term κ_P is solely a function of $c(\theta)$, while the terms κ_{PL} and $\kappa_{P\Omega}$ are functions of $c(\theta)$ and $\omega(\theta)$.

Lifting-line theory predicts that for a given wing and a given total lift coefficient, the least amount of induced-drag occurs when the lift distribution is elliptic. One way to achieve this is to have an elliptic planform shape with zero twist. An elliptic wing with no twist results in $\kappa_P = \Omega = 0$, which from Equation (9) gives

$$\left(C_{D_i}\right)_{\text{elliptic}} = \frac{C_L^2}{\pi R_A} \tag{13}$$

This is the absolute minimum induced drag a wing can produce for a given lift and wingspan [24,25,29]. Any other planform shape with zero twist will generate higher induced drag than that in Equation (13) for comparable lift coefficients and aspect ratios. Equation (13) can serve as a natural baseline for comparing the induced drag of other wing planforms and twist distributions. For a wing with an arbitrary $c(\theta)$ and $\Omega = 0$, the induced-drag coefficient from Equation (9) reduces to

$$C_{D_i} = \frac{C_L^2}{\pi R_A}(1 + \kappa_P), \qquad \kappa_P = \frac{1}{e_s} - 1 \tag{14}$$

where e_s is commonly referred to as the *span efficiency factor* [27] and κ_P is an *induced-drag planform penalty*. Examining Equations (13) and (14), we can see that κ_P is the percent increase in induced drag that a wing without twist produces compared to the elliptic wing with the same aspect ratio at the same lift coefficient. Equations (6) and (10) show that κ_P is a function of planform shape.

Figure 2 shows κ_P for various linearly tapered planforms calculated using a numerical lifting-line code [30,31]. These solutions agree closely with solutions obtained from Equations (6) and (10). Similar results for the planform penalty factor have been presented before by Glauert [32], McCormick [33], and Phillips [26,27]. Glauert's plot is the basis for the common rule of thumb that a taper ratio of about 0.5 will minimize induced drag. Results from Figure 2 show that, in the absence of twist, a taper ratio near 0.35 will minimize induced drag for most simply tapered wings over a wide range of aspect ratios. However, once twist is included, the optimum taper ratio can be significantly different.

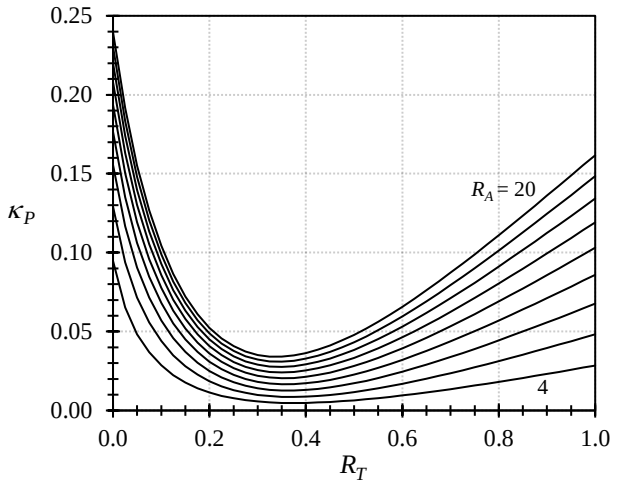


Figure 2. The induced-drag planform penalty as a function of taper ratio for a range of aspect ratios varying from 4 to 20 in increments of 2.

It has been shown that wings with arbitrary planform can produce the elliptic lift distribution and therefore produce minimum induced drag by employing the optimal twist distribution given by

$$\omega_{\text{opt}}(\theta) = 1 - \frac{\sin(\theta)}{c(\theta)/c_{\text{root}}} \tag{15}$$

$$\Omega_{\text{opt}} = -\frac{4bC_L}{\pi R_A \widetilde{C}_{L,\alpha} c_{\text{root}}} \tag{16}$$

$$(\alpha - \alpha_{L0})_{\text{root}} = \frac{C_L}{\pi R_A}\left(\frac{4b}{\widetilde{C}_{L,\alpha} c_{\text{root}}} + 1\right) \tag{17}$$

From Equations (15) and (16), we see that the optimal amount of twist depends on the lift coefficient, or flight condition, while the optimal twist distribution function is independent of operating condition and depends only on the planform shape. Since Ω depends on the flight condition, a wing with fixed twist is only optimal for one flight condition. At any other flight condition, the wing will produce a higher induced-drag coefficient than the optimum given in Equation (13). However, if a wing could continuously change the twist distribution during flight, the optimal twist distribution could be achieved for any flight condition and planform shape. The control surfaces on a wing can be used to minimize induced drag as much as possible for any given lift coefficient and planform shape. However, with a limited number of control surfaces, the absolute minimum induced drag given in Equation (13) may not be achievable. The ability of a given control-surface design to minimize drag will be called the twist effectiveness.

2.2. Twist Effectiveness

For a wing with a given $c(\theta)$, $\omega(\theta)$, and C_L, an optimal Ω can be found to minimize induced drag by taking the partial derivative of Equation (9) with respect to Ω, setting the right-hand side equal to zero, and solving for the optimal Ω. Using the optimal Ω in Equation (9) gives

$$\left(C_{D_i}\right)_{\text{opt}} = \frac{C_L^2}{\pi R_A}(1 + \kappa_{Do}), \quad \kappa_{Do} = \kappa_P - \frac{\kappa_{PL}^2}{4\kappa_{P\Omega}} \tag{18}$$

The parameter κ_{Do} is the *optimum induced-drag factor* and shows the minimum induced drag possible for a given planform and twist distribution function. It is similar to κ_P in that it is the percent increase in drag from the absolute minimum induced drag given in Equation (13) to that of a wing with a given planform, twist distribution function, and an optimum amount of twist. In other words,

$$\kappa_{Do} = \frac{\left(C_{D_i}\right)_{\text{opt}} - \left(C_{D_i}\right)_{\text{elliptic}}}{\left(C_{D_i}\right)_{\text{elliptic}}} \tag{19}$$

The term κ_{Do} is a function of both $c(\theta)$ and $\omega(\theta)$. If both of these are known, κ_{Do} can be calculated from Equations (10)–(12) and (18). Note that up to this point, no constraint has been applied to the twist distribution function and $\omega(\theta)$ is completely arbitrary. In order to compare the induced-drag performance of spanwise discrete and continuous control surfaces, the best twist distribution function possible should be used for each case. The best twist distribution function a wing can have is given in Equation (15), but this would require infinitely fine spanwise control. Realistic designs are limited by constraints on the twist distribution function and twist amount such that the twist distribution is always within the capabilities of the control mechanism. Determining an optimal twist distribution function

for a given control mechanism can be challenging. Towards this goal, κ_{Do} can be redefined into a more useful form by

$$\kappa_{Do} \equiv \kappa_P(1-\varepsilon_T), \quad \varepsilon_T = \frac{\kappa_{PL}^2}{4\kappa_{P\Omega}\kappa_P} \tag{20}$$

where ε_T is the *twist effectiveness*. The twist effectiveness, ε_T, is a measure of how well the twist distribution corrects for κ_P. The twist effectiveness can vary from 0.0 to 1.0, with 0.0 meaning that the twist cannot correct for any of the planform penalty, and 1.0 meaning that the twist can completely correct for the planform penalty.

For example, if we had a wing with a taper ratio of 1 and an aspect ratio of 18, the induced-drag planform penalty would be roughly 0.15, see Figure 2. This means that the wing without any twist will produce roughly 15% more induced drag than the optimum. However, if the twist distribution given in Equations (15) and (16) is used, $\varepsilon_T = 1$, and the control mechanism is capable of correcting for 100% of the planform penalty. If instead, the best the control mechanism was able to achieve was a twist effectiveness of 0.5, then the control mechanism would only correct for 50% of the planform penalty and the wing would produce roughly 7.5% more than the optimum, κ_{Do} = 0.075. The twist effectiveness term by itself is not enough information to determine actual changes in induced drag since it is the measure of how well the twist distribution corrects for the induced-drag planform penalty. Using Equation (20) in Equation (18) allows the induced-drag coefficient to be rewritten as

$$\left(C_{D_i}\right)_{\text{opt}} = \frac{C_L^2}{\pi R_A}[1+\kappa_P(1-\varepsilon_T)] \tag{21}$$

This formulation combines all the components of κ_{Do} dependent on twist into one parameter, ε_T, and helps in understanding and comparing the effectiveness of different control mechanisms.

2.3. Numerical Solver

For any given $c(\theta)$ and control mechanism, ε_T can be computed with the aid of aerodynamic tools and numerical optimization algorithms. Here, we use MachUp, a modern numerical lifting-line algorithm to predict the aerodynamics for a given planform and control configuration [30,31]. MachUp differs from what is commonly referred to as the numerical lifting-line algorithm [34] in that it solves for the vorticity strength at each wing section by relating the lift predicted from the section airfoil properties to the lift predicted by the three-dimensional vortex-lifting law [35], instead of enforcing a Neumann condition at the three-quarter-chord location [34]. In this regard, MachUp is more analogous of a numerical lifting-line method than that from Katz and Plotkin [34] since it uses the same fundamental relation as was used by Prandtl in classical lifting-line theory [24,25]. MachUp extends past the applicable scope of classical lifting-line by being able to model multiple lifting surfaces, each with arbitrary sweep and dihedral, even though this work considers only single wings with no sweep or dihedral. This method has shown good agreement with computational fluid dynamics solutions and experimental results for wings with aspect ratios greater than about 4 [30].

MachUp is used in conjunction with the open-source Sequential Least Squares Programming optimization algorithm [36]. The optimization algorithm calls MachUp as its objective function to determine the induced drag of the wing and allows the twist deflections to vary at the control actuation locations to minimize induced drag and maintain a given lift coefficient. For a given wing, the optimization algorithm runs multiple times for C_L values 0.5, 0.8, 1.1, and 1.4 to give a range of drag versus lift data. Then, using the κ_P values from Figure 2, Equation (21) is fit to the optimization data by varying ε_T such that

the root mean squared (RMS) of the percent error is minimized. This provides an accurate estimate of ε_T for the given wing planform and control design. For all solutions shown here, a section lift slope of 2π was used, and an RMS error less than 1.35×10^{-6} was obtained. Since the airfoil properties are modeled as linear functions without stall and since C_{D_i} is exactly proportional to C_L^2 according to lifting-line theory, the choice of C_L values for this process is somewhat arbitrary. It was found that the optimization algorithm could find solutions more effectively at higher lift coefficients where gradients are stronger. Therefore, the high lift coefficient values used here are merely a means to compute a more accurate twist effectiveness term at low angles of attack. The choice of this range of lift coefficients does not imply that anything in this work applies near or beyond stall conditions.

The analysis was only applied to a specific class of control mechanisms, even though it could be applied to others. For this class of control mechanisms, the actuators were assumed to be spaced evenly in the spanwise direction. The continuous control surfaces are modeled by having a linear variation in geometric twist between control actuators, with one always at the wing root and another always at the wing tip. Since twist is defined relative to the root, the actuator at the root determines the angle of attack of the wing. The discrete control surfaces are modeled by equally sized discrete sections of constant geometric twist. The number of sections is determined by the number of control actuators per semispan, where again the actuator at the root determines the angle of attack of the wing. Figure 1 shows an example of a four-actuator discrete and continuous control mechanism using trailing-edge flaps instead of geometric twist for clarity. The actuator deflections are equivalent between the two mechanisms shown.

This class of control mechanisms has no limits placed on the magnitudes of the control deflections. From Equation (16), we expect the magnitude of control deflections to increase with increasing lift coefficient. For a control mechanism with deflection limits, a lift coefficient will eventually be reached that saturates one or more of the control deflections from the mechanism. The twist effectiveness term is constant in the range of lift coefficients from 0 up to this saturating lift coefficient. Above this saturating lift coefficient, the twist effectiveness would vary with lift coefficient and would likely decrease. The results presented here show the cases when the control mechanism has not saturated.

3. Results

Using the process described above, ε_T can be calculated for any planform and control mechanism. This process was repeated over the range $0 \leq R_T \leq 1$ and $4 \leq R_A \leq 20$. Results are shown in Figure 3 for wings with 2–5 actuators per semispan. The reader is reminded that the twist effectiveness ε_T is a measure of how well the control mechanism can negate the drag increase caused by the planform shape. A twist effectiveness of 1.0 means that the control mechanism is 100% capable and the wing can operate at the lowest induced drag possible for that particular aspect ratio, while a twist effectiveness of 0.0 means that the control mechanism is not capable of reducing the induced drag for that wing geometry.

Notice that for both discrete and continuous control surfaces, as the number of actuators per semispan increases, the twist effectiveness improves. Recall that the twist effectiveness was defined as using the best twist distribution possible given the limitations of the control mechanism. Since a control mechanism with more degrees of freedom is better able to match the optimal solution given in Equations (15) and (16), it is expected that the twist effectiveness improves with increasing number of actuators. Also note for any given number of actuators, the continuous control surface generally has better twist effectiveness than the discrete control surface. One exception to this is the two-actuator case in the region of approximately 0.35–0.4 taper ratio, where the discrete control surface

has a very slight advantage. This range of taper ratios also appears to be a minimum-value region for the twist effectiveness for the 2–5-actuator cases. This is interesting, especially when considering Figure 2, because the taper ratio that provides the best κ_P provides the worst ε_T. One potential explanation for this is that the planform penalty is already very low, so there is less the control mechanism can do to minimize induced drag.

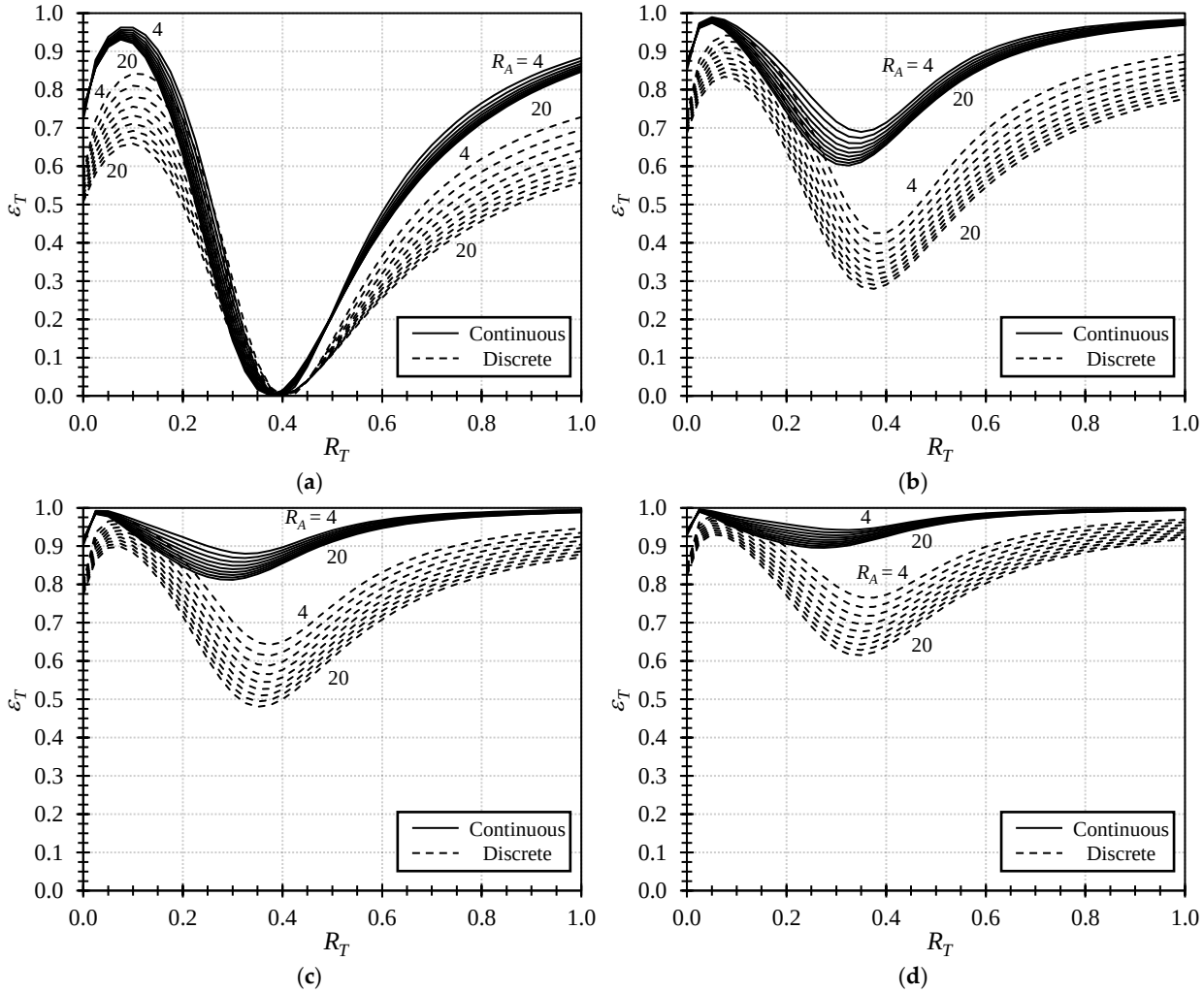


Figure 3. Twist effectiveness for a (**a**) 2-, (**b**) 3-, (**c**) 4-, and (**d**) 5-actuator control mechanism with either discrete or continuous control surfaces, shown as a function of taper ratio for aspect ratios ranging from 4 to 20 in increments of 2.

It is not uncommon to use a taper ratio near 0.5 for wings that do not use active twist to minimize induced drag. However, in light of Figure 3, if wing twist with only a few actuators is to be used to minimize induced drag, a taper ratio near 0.5 is extremely ineffective. Clearly, both the planform and control-mechanism design should be taken into account when designing a wing that actively uses the control mechanism to minimize drag.

From Equation (20), we see that κ_P and ε_T combine to give the optimum induced-drag factor, κ_{D_0}. Results for κ_{D_0} are shown in Figure 4 for different planforms and control mechanisms. Results similar to the continuous cases in Figure 4a have been presented by Phillips [26,27] in the context of a linearly tapered wing with optimal linear washout. Note that the vertical scale between the subplots in Figure 4 decreases significantly with increasing number of actuators. As expected, the more actuators used, the more closely it can produce an elliptic lift distribution. Also note that, as expected, the continuous control surfaces can nearly always outperform the discrete control surfaces for a given number of

actuators, except for the region in the two-actuator case discussed previously. However, the question arises whether the continuous control surfaces provide sufficient benefit over discrete control surfaces to offset the likely increase in manufacturing complexity and weight.

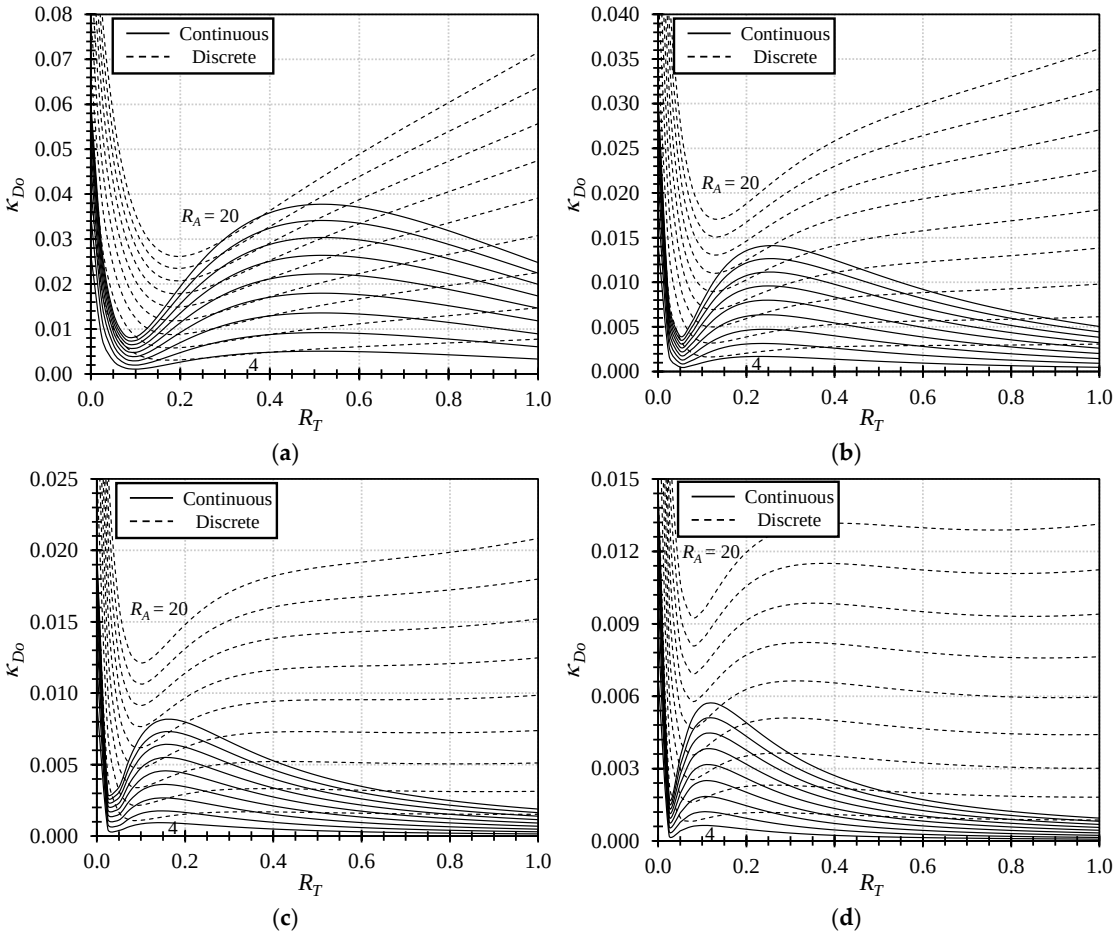


Figure 4. The term κ_{Do} for a (**a**) 2-, (**b**) 3-, (**c**) 4-, and (**d**) 5-actuator control mechanism, shown as a function of taper ratio for aspect ratios ranging from 4 to 20 in increments of 2.

It is also insightful to compare the performance of the continuous and discrete control surfaces for a given planform in terms of a percent difference in minimum induced drag between the two designs. Using the discrete control surface case as a baseline, this can be found from

$$\Delta\left(C_{D_i}\right)_{\text{opt}} \equiv \frac{\left(C_{D_i\ \text{cont}}\right)_{\text{opt}} - \left(C_{D_i\ disc}\right)_{\text{opt}}}{\left(C_{D_i\ \text{disc}}\right)_{\text{opt}}} = \frac{\kappa_{Do\ \text{cont}} - \kappa_{Do\ disc}}{1 + \kappa_{Do\ disc}} = \frac{\kappa_P\left(\varepsilon_{T\ disc} - \varepsilon_{T\ \text{cont}}\right)}{1 + \kappa_{Do\ \text{disc}}} \tag{22}$$

Results for Equation (22) are shown in Figure 5. From Figure 5, we see that a continuous control-surface design will reduce induced drag by less than 5% relative to an equivalent planform with discrete control surfaces for nearly all cases. Also note that the difference in drag between the two control surfaces diminishes with increasing number of actuators with less than 3% benefit for the three-actuator cases, less than 2% benefit for the four-actuator cases, and less than about 1% for the five-actuator cases. This is because there is an absolute minimum induced drag possible for any given aspect ratio, and as the number of actuators increase, both control-mechanism designs are better able to match the twist distribution given by Equations (15) and (16).

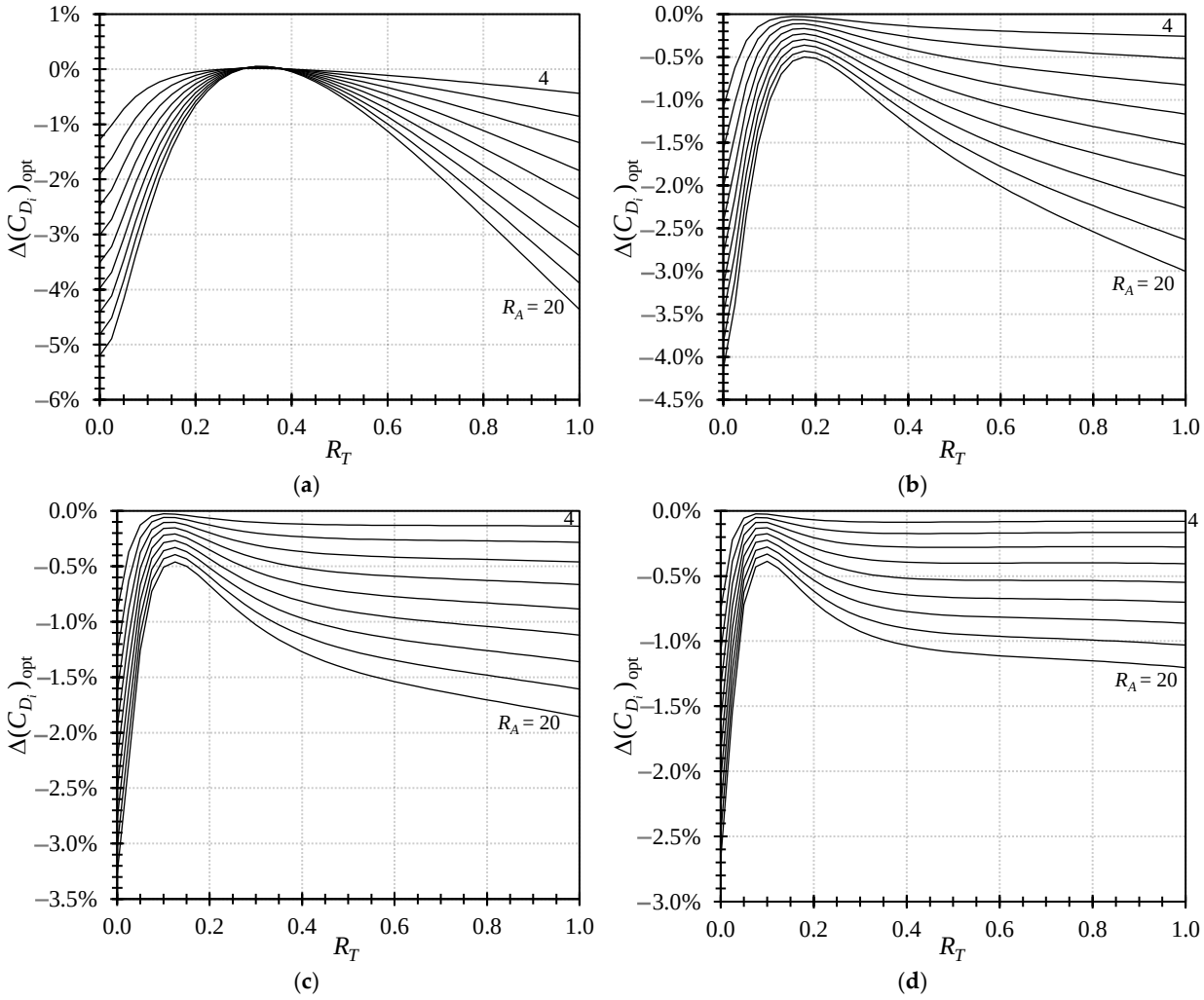


Figure 5. Percent change in induced drag of using a continuous instead of a discrete control mechanism with 2 (**a**), 3 (**b**), 4 (**c**), or 5 (**d**) actuators, shown as a function of taper ratio for aspect ratios ranging from 4 to 20 in increments of 2.

4. Discussion

A theoretical development based on lifting-line theory is presented which gives three methods for comparing the ability of continuous and discrete control surfaces to minimize induced drag. These include the twist effectiveness ε_T, the optimal induced-drag factor κ_{Do}, and a percent change in induced drag $\Delta(C_{D_i})_{\text{opt}}$. A numerical process is also presented which is capable of calculating these parameters for any given planform shape and control mechanism. This methodology was used to study discrete and continuous twist distributions on wings with evenly spaced actuators.

Wings without twist experience an induced-drag planform penalty when the planform is not elliptic. This induced-drag planform penalty is shown in Figure 2. The twist effectiveness ε_T is a measure of how well the wing's control mechanism is able to negate the induced-drag planform penalty for any given flight condition and is shown in Figure 3 for discrete and continuous control surfaces with varying number of actuators per semispan. These plots show that the continuous control surfaces generally perform better than discrete control surfaces. These results also show that, in general, control mechanisms are less effective at minimizing induced drag in the taper ratio range of 0.3–0.4. This is insightful, since this is near the taper ratio range that gives the smallest induced-drag planform penalty. Therefore, both the wing planform and control-mechanism design should be taken into

account when designing a wing that uses the control mechanism to actively reduce induced drag. Figure 3 also shows that as the number of actuators within the control mechanism increase, twist effectiveness improves. This is because higher degrees of freedom within the control mechanism, allow it to better match the optimal twist distribution given in Equations (15) and (16).

The optimal induced-drag factor κ_{D_0} combines the effects of planform and control-mechanism design and is given in Equation (20). This allows for both the induced-drag planform penalty and twist effectiveness to be considered when designing a wing. Figure 4 shows the optimal induced-drag factor which is the optimal induced drag possible for a given wing planform and control-mechanism design relative to the absolute minimum induced drag for the same aspect ratio. When viewed from this perspective, the continuous control surfaces again noticeably outperform discrete control surfaces. These results also show that the desired taper ratio is highly dependent on the control mechanism design, and that discrete control surfaces are most effective with taper ratios in the range of 0.1–0.2, while continuous control surfaces are most effective at either relatively high or low taper ratios.

The percent difference in induced drag between using a continuous and discrete control surface $\Delta\left(C_{D_i}\right)_{\text{opt}}$ can be helpful to determine whether there is sufficient aerodynamic benefit to offset the likely increase in manufacturing complexity and weight for using the continuous control surface. This percent difference is given in Equation (22), and results are shown in Figure 5. From the best case of the results presented here, wings with a continuous control surface can have an induced-drag reduction of just over 5% compared to an equivalent wing with discrete control surfaces. The difference in drag between the two control surfaces diminishes with increasing number of actuators with less than 3% benefit for the three-actuator cases, less than 2% benefit for the four-actuator cases, and less than about 1% for the five-actuator cases. This is caused by the fact that higher degrees of freedom allow the control mechanism, whether discrete or continuous, to approach the optimal solution.

The dependence of the performance of an aircraft on drag is complex. Therefore, a blanket statement about how a reduction in drag would affect the overall performance of aircraft is difficult to make. However, it is insightful that a 5% reduction in induced drag can roughly be correlated with a 2.5% reduction in thrust, if induced drag was originally 50% of the total drag. This could translate to about a 2.5% reduction in fuel required, which would lower the weight of the aircraft and reciprocally result in further drag reduction.

Continuous control surfaces, in general, have greater aerodynamic efficiency capabilities than discrete control surfaces. However, the ideal aerodynamic benefits for induced drag shown in this study are small. It should be noted that lifting-line theory used here to determine the ideal aerodynamics does not take into account any flow spillage that may occur across the gap created by two adjacent discrete control surfaces that have different deflections. Accounting for this would likely cause the discrete control surfaces to have more drag than shown here. Future work could include comparing efficiencies of spanwise discrete and continuous control surfaces while taking into account parasitic drag and the discrete control surface flow spillage effect.

As a final note, the present manuscript includes two main contributions. The first is simply a method for comparing the effectiveness of discrete control surfaces to continuous. The method followed here could be repeated using wind-tunnel experiments, computational fluid dynamics, or higher-fidelity aerodynamic prediction methods. The second contribution is the presentation of results of this method based on lifting-line theory. The limitations of lifting-line theory are well documented in the literature. As a reminder, the results shown here neglect influence of viscosity, and should not be expected to be accurate

for wings with aspect ratios less than about 4. Additionally, compressibility effects have been neglected. Nevertheless, the trends obtained from these results are insightful and can guide the discussion and development of future morphing-wing controls.

Author Contributions: Conceptualization, Z.S.M. and D.F.H.; methodology, Z.S.M. and D.F.H.; software, Z.S.M.; validation, Z.S.M.; formal analysis, Z.S.M.; investigation, Z.S.M.; resources, D.F.H.; data curation, Z.S.M.; writing—original draft preparation, Z.S.M.; writing—review and editing, Z.S.M. and D.F.H.; visualization, Z.S.M.; supervision, D.F.H. and J.J.J.; project administration, D.F.H. and J.J.J.; funding acquisition, D.F.H. and J.J.J. All authors have read and agreed to the published version of the manuscript.

Funding: This work was funded by the Air Force Office of Scientific Research (AFOSR) Lab Task 17RQCOR394 with Dr. Jay Tiley as the program manager and by the U.S. Office of Naval Research Sea-Based Aviation program (Grant No. N00014-18-1-2502) with Brian Holm-Hansen as the program officer. This paper has been cleared for public release, Case Number: 88ABW-2020-2554.

Data Availability Statement: The original contributions presented in this study are included in the article. Further inquiries can be directed to the corresponding author.

Acknowledgments: The contents of this article were originally presented as part of paper 2020–2008 at the AIAA SciTech 2020 Forum, Orlando, Florida, 6–10 January 2020 [37].

Conflicts of Interest: The authors declare no conflicts of interest. The funders had no role in the design of the study; in the collection, analyses, or interpretation of data; in the writing of the manuscript; or in the decision to publish the results.

Nomenclature

A_n	coefficient in the Fourier sine series
a_n	decomposed Fourier coefficient relating to angle of attack
b	wingspan
b_n	decomposed Fourier coefficient relating to wing twist
C_{D_i}	Induced-drag coefficient
C_L	lift coefficient
$C_{L,\alpha}$	lift slope
$\widetilde{C}_{L,\alpha}$	local airfoil lift slope
c	local chord length
e_s	spanwise efficiency factor
N	number of terms retained from the infinite Fourier sine series
n	index for the Fourier sine series
R_A	aspect ratio
R_T	taper ratio
T	twist at a spanwise position of the wing
V_∞	freestream velocity
z	spanwise coordinate, positive out the left wing
α	geometric angle of attack of an airfoil at a spanwise position
α_{L0}	zero-lift angle of attack of an airfoil at a spanwise position
Γ	vortex strength at a spanwise position along the lifting line
ε_T	twist effectiveness
θ	change in variable for the spanwise coordinate
κ_{Do}	optimum induced-drag factor
κ_P	induced-drag planform penalty
κ_{PL}	lift-twist contribution to induced drag
$\kappa_{P\Omega}$	twist contribution to induced drag

Ω	amount of twist, determines the amount and direction of wing twist but not the shape
ω	twist distribution function, determines the shape of the twist distribution

References

1. Glines, C.V. The Promise of Flight Fulfilled. *Aviat. Hist.* **2003**, *14*, 26.
2. Lougheed, V.V. The Secret Experiments of the Wright Brothers Victor Longhand, Popular Mechanics. In *Popular Mechanics*; Hearst Corporation: New York, NY, USA, 1911; pp. 797–804.
3. Marks, C.R.; Zientarski, L.; Culler, A.J.; Hagen, B.; Smyers, B.M.; Joo, J.J. Variable Camber Compliant Wing—Wind Tunnel Testing. In Proceedings of the AIAA 2015-1051, 23rd AIAA/AHS Adaptive Structures Conference, Kissimmee, FL, USA, 5–9 January 2015.
4. Kaul, U.K.; Nguyen, N.T. Drag Optimization Study of Variable Camber Continuous Trailing Edge Flap (VCCTEF) Using OVERFLOW. In Proceedings of the 32nd AIAA Applied Aerodynamics Conference, Atlanta, GA, USA, 16–20 June 2014.
5. Lebofsky, S.; Ting, E.; Nguyen, N.T.; Trinh, K.V. Aeroelastic Modeling and Drag Optimization of Flexible Wing Aircraft with Variable Camber Continuous Trailing Edge Flap. In Proceedings of the 32nd AIAA Applied Aerodynamics Conference, Atlanta, GA, USA, 16–20 June 2014.
6. Ting, E.; Dao, T.; Nguyen, N.T. Aerodynamic Load Analysis of a Variable Camber Continuous Trailing Edge Flap System on a Flexible Wing Aircraft. In Proceedings of the 56th AIAA/ASCE/AHS/ASC Structures, Structural Dynamics, and Materials Conference, Kissimmee, FL, USA, 5–9 January 2015.
7. Nguyen, N.; Urnes, J. Aeroelastic Modeling of Elastically Shaped Aircraft Concept via Wing Shaping Control for Drag Reduction. In Proceedings of the AIAA Atmospheric Flight Mechanics Conference, Minneapolis, MN, USA, 13–16 August 2012.
8. Kudva, J.; Appa, K.; Martin, C.; Jardine, A.; Sendeckyj, G.; Harris, T.; McGowan, A.; Lake, R. Design, Fabrication, and Testing of the DARPA/Wright Lab Smart Wing Wind Tunnel Model. In Proceedings of the AIAA-1997-1198, 38th Structures, Structural Dynamics, and Materials Conference, Kissimmee, FL, USA, 7–10 April 1997.
9. Gilbert, W.W. Development of a Mission Adaptive Wing System for a Tactical Aircraft. In Proceedings of the Aircraft Systems Meeting, Aircraft Design and Technology Meeting, Anaheim, CA, USA, 4–6 August 1980.
10. Hall, J.M. *Executive Summary AFTI/F-111 Mission Adaptive Wing*; WRDC-TR-89-2083; Wright Research and Development Center: Dayton, OH, USA, 1989.
11. Hetrick, J.; Osborn, R.; Kota, S.; Flick, P.; Paul, D. Flight Testing of Mission Adaptive Compliant Wing. In Proceedings of the AIAA-2007-1709, 48th AIAA/ASME/ASCE/AHS/ASC Structures, Structural Dynamics, and Materials Conference, Honolulu, HI, USA, 23–26 April 2007.
12. Vos, R.; Gurdal, Z.; Abdalla, M. Mechanism for Warp-Controlled Twist of a Morphing Wing. *J. Aircr.* **2010**, *47*, 450–457. [CrossRef]
13. Dale, A.S.; Cooper, J.E.; Mosquera, A. Adaptive Camber-Morphing Wing using 0-υ Honecomb. In Proceedings of the AIAA-2013-1510, 54th AIAA/ASME/ASCE/AHS/ASC Structures, Structural Dynamics, and Materials Conference, Boston, MA, USA, 8–11 April 2013.
14. Molinari, G.; Arrieta, A.F.; Guillaume, M.; Ermanni, P. Aerostructural Performance of Distributed Compliance Morphing Wings: Wind Tunnel and Flight Testing. *AIAA J.* **2016**, *54*, 3859–3871. [CrossRef]
15. Lyu, Z.; Martins, J.R.R.A. Aerodynamic Shape Optimization of an Adaptive Morphing Trailing-Edge Wing. *J. Aircr.* **2015**, *52*, 1951–1970. [CrossRef]
16. Fasel, U.; Tiso, P.; Keidel, D.; Molinari, G.; Ermanni, P. Reduced-Order Dynamic Model of a Morphing Airborne Wind Energy Aircraft. *AIAA J.* **2019**, *57*, 3586–3598. [CrossRef]
17. Previtali, F.; Arrieta, A.F.; Ermanni, P. Performance of a Three-Dimensional Morphing Wing and Comparison with a Conventional Wing. *AIAA J.* **2014**, *52*, 2101–2113. [CrossRef]
18. Wickenheiser, A.M.; Garcia, E. Aerodynamic Modeling of Morphing Wings Using an Extended Lifting-Line Analysis. *J. Aircr.* **2007**, *44*, 10–16. [CrossRef]
19. Gamboa, P.; Vale, J.; Lau, F.J.P.; Suleman, A. Optimization of a Morphing Wing Based on Coupled Aerodynamic and Structural Constraints. *AIAA J.* **2009**, *47*, 2087–2104. [CrossRef]
20. Molinari, G.; Arrieta, A.F.; Ermanni, P. Aero-Structural Optimization of Three-Dimensional Adaptive Wings with Embedded Smart Actuators. *AIAA J.* **2014**, *52*, 1940–1951. [CrossRef]
21. Béguin, B.; Breitsamter, C.; Adams, N. Aerodynamic Investigations of a Morphing Membrane Wing. *AIAA J.* **2012**, *50*, 2588–2599. [CrossRef]
22. Keidel, D.; Fasel, U.; Ermanni, P. Concept Investigation of a Lightweight Composite Lattice Morphing Wing. *AIAA J.* **2021**, *59*, 2242–2250. [CrossRef]
23. Burdette, D.A.; Martins, J.R.R.A. Impact of Morphing Trailing Edges on Mission Performance for the Common Research Model. *J. Aircr.* **2019**, *56*, 369–384. [CrossRef]

24. Prandtl, L. Tragflügel Theorie. Nachricten von der Gesellschaft der Wissenschaften zu Gottingen. *Geschäeftliche-Mitteilungen Kl.* **1918**, *1918*, 451–477.
25. Prandtl, L. *Applications of Modern Hydrodynamics to Aeronautics*; NACA TR-116; NASA: Washington, DC, USA, 1921.
26. Phillips, W.F. Lifting-Line Analysis for Twisted Wings and Washout-Optimized Wings. *J. Aircr.* **2004**, *41*, 128–136. [CrossRef]
27. Phillips, W.F. *Incompressible Flow over Finite Wings. Mechanics of Flight*, 2nd ed.; Wiley: Hoboken, NJ, USA, 2010; pp. 46–94.
28. Phillips, W.F. Analytical Decomposition of Wing Roll and Flapping Using Lifting-Line Theory. *J. Aircr.* **2014**, *51*, 761–778. [CrossRef]
29. Phillips, W.F.; Hunsaker, D.F.; Taylor, J.D. Minimizing Induced Drag with Weight Distribution, Lift Distribution, Wingspan, and Wing-Structure Weight. In Proceedings of the AIAA Aviation 2019 Forum, Dallas, TX, USA, 17–21 June 2019.
30. Phillips, W.F.; Snyder, D.O. Modern Adaptation of Prandtl's Classic Lifting-Line Theory. *J. Aircr.* **2000**, *37*, 662–670. [CrossRef]
31. Hodson, J.; Hunsaker, D.F.; Spall, R. Wing Optimization Using Dual Number Automatic Differentiation in MachUp. In Proceedings of the 55th AIAA Aerospace Sciences Meeting, AIAA SciTech Forum, Grapevine, TX, USA, 9–13 January 2017.
32. Glauert, H. *The Elements of Aerofoil and Airscrew Theory*; Cambridge University Press: London, UK, 1926.
33. McCormick, B.W. *Numerical Model of a Lifting Line to Determine Induced Drag. Aerodynamics, Aeronautics, and Flight Mechanics*, 2nd ed.; John Wiley & Sons: Hoboken, NJ, USA, 1995; pp. 171–174.
34. Katz, J.; Plotkin, A. Lifting-Line solution by horseshoe elements. In *Low-Speed Aerodynamics*, 2nd ed.; Cambridge University Press: New York, NY, USA, 2001.
35. Saffman, P.G. *; Vortex Dynamics*; Cambridge University Press: Cambridge, UK, 1992. [CrossRef]
36. Kraft, D. *A Software Package for Sequential Quadratic Programming*; Tech. Rep, DFVLR-FB 88-28; DLR German Aerospace Center—Institute for Flight Mechanics: Koln, Germany, 1988.
37. Montgomery, Z.S.; Hunsaker, D.F.; Joo, J.J. Aerodynamic Efficiency Analysis of Morphing Wings Relative to Non-Morphing Wings. In Proceedings of the AIAA 2020-2008, AIAA Scitech 2020 Forum, Orlando, FL, USA, 6–10 January 2020.

Disclaimer/Publisher's Note: The statements, opinions and data contained in all publications are solely those of the individual author(s) and contributor(s) and not of MDPI and/or the editor(s). MDPI and/or the editor(s) disclaim responsibility for any injury to people or property resulting from any ideas, methods, instructions or products referred to in the content.